The contribution from transit dose for ^{192}Ir HDR brachytherapy treatments

2014 Phys. Med. Biol. 59 1831

(http://iopscience.iop.org/0031-9155/59/7/1831)

IOP Publishing | Institute of Physics and Engineering in Medicine Physics in Medicine and Biology

Phys. Med. Biol. **59** (2014) 1831–1844 doi:10.1088/0031-9155/59/7/1831

The contribution from transit dose for ^{192}Ir HDR brachytherapy treatments

G P Fonseca[1,2], G Landry[2], B Reniers[2], A Hoffmann[2], R A Rubo[3], P C G Antunes[1], H Yoriyaz[1] and F Verhaegen[2,4]

[1] Instituto de Pesquisas Energéticas e Nucleares—IPEN-CNEN/SP, São Paulo, Brazil
[2] Department of Radiation Oncology (MAASTRO), GROW School for Oncology and Developmental Biology, Maastricht University Medical Center, Maastricht 6201 BN, The Netherlands
[3] Hospital das Clínicas da Universidade de São Paulo—HC/FMUSP, São Paulo, Brazil
[4] Medical Physics Unit, Department of Oncology, McGill University, Montréal, Québec H3G 1A4, Canada

E-mail: frank.verhaegen@maastro.nl

Received 20 October 2013, revised 5 February 2014
Accepted for publication 18 February 2014
Published 14 March 2014

Abstract

Brachytherapy treatment planning systems that use model-based dose calculation algorithms employ a more accurate approach that replaces the TG43-U1 water dose formalism and adopt the TG-186 recommendations regarding composition and geometry of patients and other relevant effects. However, no recommendations were provided on the transit dose due to the source traveling inside the patient. This study describes a methodology to calculate the transit dose using information from the treatment planning system (TPS) and considering the source's instantaneous and average speed for two prostate and two gynecological cases. The trajectory of the ^{192}Ir HDR source was defined by importing applicator contour points and dwell positions from the TPS. The transit dose distribution was calculated using the maximum speed, the average speed and uniform accelerations obtained from the literature to obtain an approximate continuous source distribution simulated with a Monte Carlo code. The transit component can be negligible or significant depending on the speed profile adopted, which is not clearly reported in the literature. The significance of the transit dose can also be due to the treatment modality; in our study interstitial treatments exhibited the largest effects. Considering the worst case scenario the transit dose can reach 3% of the prescribed dose in a gynecological case with four catheters and up to 11.1% when comparing the average prostate dose for a case with 16 catheters. The transit dose component increases by increasing the number of catheters used for HDR brachytherapy, reducing the total dwell time per catheter or increasing the number of dwell positions with low dwell times. This contribution may become significant

(>5%) if it is not corrected appropriately. The transit dose cannot be completely compensated using simple dwell time corrections since it may have a non-uniform distribution. An accurate measurement of the source acceleration and maximum speed should be incorporated in clinical practice or provided by the manufacturer to determine the transit dose component with high accuracy.

Keywords: transit dose, HDR, ^{192}Ir, MBDCA, Monte Carlo

(Some figures may appear in colour only in the online journal)

1. Introduction

Brachytherapy treatment planning systems (TPS) that adopt TG-186 (Beaulieu *et al* 2012) recommendations use model-based dose calculations algorithms (MBDCA) that are capable of handling tissue compositions, use density maps from computed tomography (CT) and handle applicators surpassing the TG-43U1(Nath *et al* 1995, Rivard *et al* 2004) homogeneous water dose formalism. Several MBDCA software packages have been developed; the commercial ACUROS^{TM} (Transpire, Inc., Gig Harbor, WA (Petrokokkinos *et al* 2011)) which employs a grid-based Boltzmann solver, and several in-house Monte Carlo (MC)-based algorithms (Afsharpour *et al* 2012, Poon *et al* 2008).

The transit dose component can be relevant due to the source slowing down near the dwell positions and should be considered, especially for sources with high air-kerma strengths where transit times are relatively higher when compared to dwell times, and for treatments with several dwell positions and catheters where the source spends a significant amount of time in transit (Fonseca *et al* 2013).

This paper describes a methodology that uses the information extracted from the treatment plan to define the source trajectory creating a continuous source distribution where the sampling probability at each position was weighted by the source speed extracted from the literature (Minamisawa *et al* 2010, Palmer and Mzenda 2009, Wojcicka *et al* 1999).

The instantaneous or even the average source speed measurement is a relevant issue since this parameter is not well known with reported differences up to a factor 10 depending on the measurement methodology. Table 1 presents an overview of the literature data with results obtained using a video camera (Wong *et al* 2001, Palmer and Mzenda 2009), ionization chamber (Sahoo 2001), optical fibers to detect Cerenkov induced effect (Minamisawa *et al* 2010), film analysis (Wojcicka *et al* 1999), and also manufacturer information without describing the adopted methodology (Bastin *et al* 1993). Three of those studies found that the source follows a uniformly accelerated movement for the Nucletron afterloader with different accelerations reported $|a| = 113$ cm s^{-2} (Minamisawa *et al* 2010) and $|a| = 78$ cm s^{-2} (Wojcicka *et al* 1999); for the Varian afterloader $|a| = 55$ cm s^{-2} (Wojcicka *et al* 1999), and for the Eckert & Ziegler BEBIG GmbH MultiSource (^{192}Ir HDR) afterloader $|a| = 77$ cm s^{-2} (Palmer and Mzenda 2009).

Most of the measured results do not agree with the manufacturer's specifications since most of the data provided by the manufacturers are referring to the source moving from the afterloader to the first dwell position and returning back to it from the last well position, which may not represent the source speed between the dwell positions. Nucletron, Varian and BEBIG quote average speeds of 50, 60 and 30 cm s^{-1}, respectively (Venselaar 2013). Differences in the speed profile can lead to significant differences in the transit dose component, which were evaluated in the present study for four clinical cases from three different centers, which were simulated using a general multipurpose MC code, MCNP5 (Monte Carlo N-Particle Transport

Table 1. Average source speed between dwell positions for various inter-dwell distances (d_{id}) reported in the literature for afterloaders from Nucletron (microSelectron), Varian (GammaMed-Plus) and for Eckert & Ziegler BEBIG GmbH MultiSource (^{192}Ir HDR).

	Average source speed (cm s^{-1})							
	Nucletron—microSelectron						Varian GammaMed-Plus	BEBIG ^{192}Ir HDR
d_{id} (cm)	Wong	Sahoo	Bastin	Houdek	Minamisawa[a]	Wojcicka[a]	Wojcicka[a]	Palmer[a]
0.25	5.4	–	–	22.7	2.7	2.2	1.9	2.2
0.50	7.2	33.3	23.0	27.1	3.8	3.1	2.6	3.1
1.00	23.3	50.0	25.5	30.3	5.3	4.4	3.7	4.4
2.00	–	80.0	–	–	7.5	6.2	5.2	6.2
3.00	–	60.0	–	–	9.2	7.6	6.4	7.6
4.00	–	42.1	–	–	10.6	8.8	7.4	8.8

[a] Values calculated using the uniform acceleration approach.

code, version 5) (Briesmeister 2008). The cases include two prostate and two gynecological cases that were evaluated to provide a general overview.

Although MBDCA have a more accurate dose calculation engine than the currently available water-based TG43-U1 based TPS, they do not include the transit dose component due to the source travel.

2. Materials and methods

2.1. Geometry definition

The dwell positions and the catheter contours can be imported from the BrachyVision™ (Varian, Palo Alto, CA) and the Oncentra™ (Elekta AB, Stockholm, Sweden) TPS, consisting of point coordinates related to the treatment plan geometry. These points were used to define the trajectory of the source inside the patient and its inclination. The length of the catheter and the number of contour points depend on the catheter contouring process and the number of segments created to define the source trajectory in the treatment plan, or, alternatively, on the method of defining the applicator in the TPS applicator library. The catheter points and the dwell positions were processed using an algorithm created with MATLAB version 8.0 (Mathworks Inc., Natick, MA, USA), which provides the trajectory of the source, the speed at each reference position, control points where the acceleration changes direction, the source orientation and the time necessary to travel between two consecutive points for both the source going into the patient and coming back to the safe.

The trajectory depends on the treatment plan and is mainly restricted to the region near to the target volume since the catheters outside the body, in general, are not defined when planning. However, this is not a limitation for this study since its main interest is the transit dose due to the source travel between dwell positions, with a low speed near the dwell positions as shown in section 2.3.1.

2.2. Monte Carlo dose calculations

The transit dose distribution due to the source traveling inside the patient, without considering the dwell time, and the dwell dose distribution were obtained separately for four clinical cases using the MCNP5 MC code. The simulations used the ^{192}Ir National Nuclear Data Center (NNDC) photon emission spectrum, and transported photons with an energy cut-off

of 1 keV, using the MCPLIB84 photon cross-section library (Wong *et al* 2001). Since the goal was to analyze the transit dose component and the effect of several speed profiles, all the cases were simulated under the same conditions using a MicroSelectron v.2 source that was validated by simulating TG43-U1 parameters in a 30 cm diameter water phantom following the methodology proposed by Daskalov *et al* (1998). This approach ensures that differences between the cases are not due to the source model. The simulations were performed with 10^9 photons resulting in a dose uncertainty component type A ($k = 1$) of less than 1.5% for points with a dose higher than 10% of the prescribed dose.

2.3. Transit dose calculation

The transit dose and the dwell dose were evaluated using a phase space file, which was generated on the surface of the stainless steel capsule encasing the ^{192}Ir isotope considering a 2 mm long cable. The MC transit dose calculations for the clinical cases simulate the source at discrete positions every 10 μm following the source trajectory with a sampling probability defined as the inverse of the instantaneous speed along the trajectory, which is proportional to the time spent by the source to travel within each 10 μm segment for the source going into the patient, traveling between the dwell positions and coming back to the safe. The discrete methodology should be equivalent to a continuous distribution due to the high spatial resolution adopted, which was evaluated using a continuous and a discrete distribution for a point source following a straight trajectory. This methodology was employed in a previous study (Fonseca *et al* 2013) where simulated data were also validated by comparison against experimental values obtained by Calcina *et al* (2005).

This study adopted a maximum source instantaneous speed of 52 cm s^{-1} (Minamisawa *et al* 2010) with the instantaneous source speed at each position calculated using reference speeds and accelerations from the literature following the three approaches: (a) uniform acceleration; (b) an average speed obtained considering the inter-dwell distance and the travel time, which was obtained using the source acceleration; (c) the average speed of 30 and 50 cm s^{-1} specified by two manufacturers. The average speed values provided by the manufacturers do not depend on the inter-dwell distance and may not refer to the speed between the dwell positions, depending on the measurement methodology, although these speed values can be used as reference values. Nucletron suggests dwell time corrections using an average speed of 50 cm s^{-1} for a 5 mm inter-dwell distance (Planning system manual).

2.3.1. Validation. The MC source distribution for the clinical cases simulates the source at each position, which is equivalent to the superposition principle used to validate simulation results for simplified cases. While the studied cases were evaluated accounting for the anisotropy, scattering and other interactions, the validation process was performed using an isotropic point source and the superposition technique, which can be verified with simple dose calculation algorithms. The validation process consists of three steps:

(a) speed profile verification by comparing the speed profile calculated using the TPS contour information and obtained analytically;
(b) MC simulation of the transit dose component versus a calculation using MATLAB for a treatment plan created for a point source and a linear 10 cm long catheter with dwell positions distributed uniformly along it for inter-dwell distances of 2.5, 5.0, 10.0 and 20 mm. This is illustrated in figure 1 for a simplified case with three dwell positions;
(c) creation of a treatment plan for a ring applicator with 32 mm diameter defined in the BrachyVision^{TM} applicators library (ref: AL13017000) with inter-dwell distance of 0.5 cm

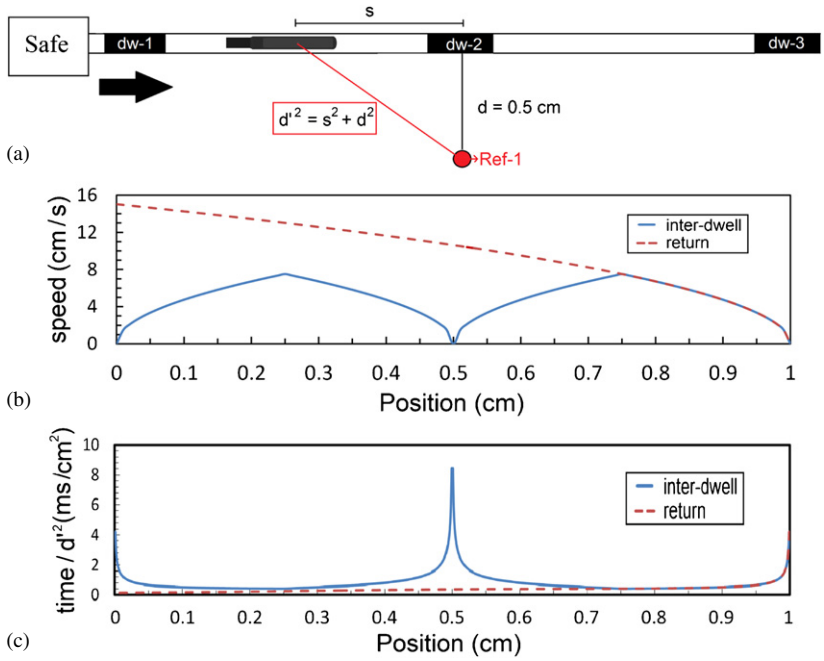

Figure 1. (a) Source moving between three dwell positions with inter-dwell distance of 0.5 cm; (b) source speed profile for a uniform accelerated movement; (c) contribution of each source position to transit dose at the reference point due the source traveling between the dwell positions and returning to the safe.

used only to verify the source trajectory. The transit dose distribution was simulated considering the source instantaneous speed, and then exported back to the TPS as DICOM images allowing a visualization of the applicator and the dwell positions superimposed over the transit dose distribution.

The transit dose component for one reference point (ref-1) figure 1(a) was estimated considering a trajectory composed by N steps of 10 μm with travel times calculated using a source instantaneous speed profile (figure 1(b)). The contribution of each step along the trajectory to the total transit dose at the reference point (ref-1) is proportional to the travel time of each step weighted by the square of the distance d' between the position of the center of the 10 μm step and the reference point to take into account the inverse-square law, resulting in the distribution presented in figure 1(c). Finally, the transit dose component (D_{tr}) was obtained by integrating the obtained distribution and multiplying it by the dose rate $\left(\dot{D}\right)$ for an arbitrary reference distance (d_{ref}) as described in the following equation, which was used to validate the MC results obtained and to evaluate a possible correction:

$$D_{\mathrm{tr}} = \dot{D} \cdot d_{\mathrm{ref}}^2 \sum_{i=1}^{N} \frac{t_i}{d_i'^2}. \tag{1}$$

This approach considers only the square distance law, although it is a reasonable approach for a simple case validation since a point source was adopted to eliminate anisotropy functions and the scattered photons have a much smaller effect than the square law for positions close to the source.

2.3.2. Dwell time correction. The transit dose contribution to the total dose can be compensated by decreasing the dwell time, as currently applied by some manufacturers, using simple approaches that divide the inter-dwell travel distance by the average source speed reducing the dwell time up to 0.1 s per dwell position for the Nucletron afterloader, considering the travel time from the last position up to the current position as part of the dwell time for the GammaMed iX afterloader and using the following equation for the BEBIG afterloader (Palmer and Mzenda 2009):

$$\mathrm{pDT} = (\mathrm{DT} - T_{r(\text{to dwell})} - T_{r(\text{from dwell})}) \quad T_r = (cd_{\mathrm{id}} + 100) \times 10^{-3} \tag{2}$$

where pDT is the corrected dwell time (s), DT (s) is the dwell time without correction and T_r (s) the correction time obtained using the inter dwell distance (d_{id}) in mm, considering the source coming to the dwell position (to dwell) and the source leaving the dwell position (from dwell), multiplied by a constant c (3 s mm^{-1} for inter-dwell distance less than or equal to 10 mm and 2 s mm^{-1} for greater distances) and adding 100 s. Equation (2) was adopted by Palmer and Mzenda (2009), but the methodology used to obtain this equation has not been described.

To the best of our knowledge there is no algorithm to correct the transit dose based on the instantaneous source speed that takes the acceleration into account. In an attempt to reduce the transit dose effect, the transit dose (D_{tr}) was calculated for several inter-dwell distances (from 0.25 cm up to 10 cm) considering four reference points defined along a line orthogonal to the source longitudinal axis and at distances d (0.25, 0.5, 1 and 2 cm) as illustrated for one reference point (ref-1) in figure 1(a). Finally, the correction time for the nearest dwell position to compensate the transit dose was calculated for each reference point leading to the following empirical equation:

$$T_c = \frac{1}{2}\sqrt{\frac{113}{a}}\left(T_{r'(\text{to dwell})} + T_{r'(\text{from dwell})} + T'_{\text{return}}\right) \tag{3}$$

$$\begin{aligned} T_{r'} &= +0.0261 \ln\left(d_{\mathrm{id}}/d_{\mathrm{ref}}\right) + 0.1241 \quad \text{for} \quad d_{\mathrm{id}} \leqslant 15 \text{ mm} \\ T_{r'} &= +0.1355 \quad \text{for} \quad d_{\mathrm{id}} > 15 \text{ mm} \\ T'_{\text{return}} &= -0.0011\left(d_{lp}/d_{\mathrm{ref}}\right) + 0.1220 \end{aligned}$$

where the correction time (T_c) in s, that should be subtracted from the TPS dwell time of the nearest dwell position. T_c depends on the reference distance (d_{ref}), 1 mm, the inter-dwell distances (d_{id}) in mm and the distance between the current and the last position $\left(d_{lp}\right)$ in mm.

Equation (3) includes the source coming from the previous position or from the safe to the current dwell position, $T_{r'(\text{todwell})}$ in s. The latter is approximated as an inter-dwell distance of 100 mm, T_c also depends on the source going from the current position to the next dwell position, $T_{r'(\text{fromdwell})}$ in s, and the source returning to the safe, T'_{return} in s. The factor 1/2 was included since the transit time in one inter-dwell segment will be corrected for two consecutive dwell positions and the factor $(113/a)^{1/2}$ includes the acceleration effect since the time of each discrete step is inversely proportional to the square root of the ratio of the reference acceleration (113 cm s^{-2}) and the acceleration (a) as obtained from kinematics and evaluated for accelerations (a) between 10 and 200 cm s^{-2} to cover the literature data interval.

The described approach compensates the transit dose effect, includes the acceleration and preserves the simplicity of the manufacturer's approaches. Although our approach includes the acceleration component, with the currently available algorithms it cannot completely correct the transit dose due to the limited number and location of the dwell positions. Moreover, complex transit dose distributions may occur, e.g. due to different inter-dwell distances in the same setup and/or due to the geometry and the number of catheters.

2.4. Clinical cases

Two gynecological cases and one prostate case were planned for a microSelectron-HDR ^{192}Ir source (Daskalov *et al* 1998) using the TG-43U1 dose while one prostate case was planned for a GamammedPlus source (Taylor *et al* 2008). These cases were selected to provide a general overview of the transit dose component since they differ considerably in the number of catheters, inter-dwell distance and geometry. Regardless of the differences between the source, all the cases were simulated using the microSelectron-HDR source with the dwell times of each case scaled to an air-kerma strength of 40 700 U in order to evaluate all cases under the same air-kerma strength and also to evaluate the worst case scenario since the transit dose is directly proportional to this parameter. Simulations were performed for two situations: (a) an infinite water medium, which was created by adding at least 20 cm of water at each side of the body (Perez-Calatayud *et al* 2004); (b) a heterogeneous medium composed of five materials, air (mass density $\rho = 0.0012\,041$ g cm^{-3}), water ($\rho = 1.0$ g cm^{-3}), adipose tissue ($\rho = 0.92$ g cm^{-3}), muscle ($\rho = 1.06$ g cm^{-3}) and cortical bone ($\rho = 1.85$ g cm^{-3}) defined using Hounsfield units (HU) with compositions defined by ICRP (1975). One density was specified for each material to assure that MCNP5 uses the same composition and density specified using ACUROS^{TM} (Transpire, Inc., Gig Harbor, WA), a grid-based Boltzmann solver, which was used, in a parallel work, to validate the dose distributions without the transit dose. The cases were compared considering the 3D dose distributions and also by comparing doses at prescription points defined by the physician responsible for the case, since structure contours were not created for all cases.

$D_{w,m}$ (dose to water in medium) values were obtained for all cases and only the values obtained for an infinite water phantom are presented, except when stated otherwise, since the transit dose component relative to the dwell dose is the same for all the conditions evaluated.

2.4.1. Gynecological cases. Two gynecological cases differing significantly in the number of needles and dwell positions were selected to evaluate the impact of the number of needles and their locations. The evaluated cases were: case (a) a treatment performed with a hollow cylindrical vaginal applicator with an external diameter of 35 mm and a polysulfone wall of 4 mm with one 12 cm long needle in the center totaling 17 dwell positions, inter-dwell distance of 2.5 mm and a total dwell time of 405 s. The reference points were defined at a distance of 5 mm from the right hand side of the applicator wall with an average dose of 7 Gy; case (b) a treatment performed with the same applicator described in the previous case using the central needle of the applicator and three needles distributed near the lower surface of the applicator totaling 100 dwell positions and a total dwell time of 556 s. Each needle has been defined during the treatment planning with approximately 12 cm of contour length and an inter-dwell distance of 2.5 mm. The reference dose points were defined on the right hand side of the applicator's surface with an average dose of 15 Gy.

2.4.2. Prostate cases. Two prostate cases were selected, which had approximately the same total dwell time and prescribed dose, but a significantly different number and distribution of the needles. The evaluated cases were: case (c) a treatment performed using 16 flexible catheters with lengths defined through contours during the planning between 3.8 and 6.3 cm, the number of dwell positions varying from 2 up to 8 depending on the catheter, and distances between active positions from 0.5 up to 2 cm totaling 113 dwell positions with a total dwell time of 200.9 s. The prescribed dose at the surface of the prostate was 10 Gy; case (d) a treatment performed using seven catheters with lengths defined through contours during the planning between 5.3 and 9.6 cm, number of dwell positions varying from 6 up to 8 depending

Table 2. Transit dose for a reference point orthogonal to the catheter's longitudinal axis and positioned at 0.5 cm from its center (figure 1(a)). The values were calculated analytically (An.) and simulated (MC) extracting the information from a treatment plan created with BrachyVision™. The underlined speeds were obtained considering a uniform accelerated movement for an acceleration of 113 cm s^{-2} (Nucletron (Minamisawa *et al* 2010)) and 55 cm s^{-2} (Varian (Wojcicka *et al* 1999)).

Inter-dwell distance (cm)												
0.25			0.5			1			2		
	Dose (cGy)			Dose (cGy)			Dose (cGy)			Dose (cGy)	
v (cm s^{-1})	An.	MC	v (cm s^{-1})	An.	MC	v (cm s^{-1})	An.	MC	v (cm s^{-1})	An.	MC
60.0	2.5	2.5	60.0	2.5	2.5	60.0	2.5	2.5	60.0	2.5	2.5
30.0	5.0	5.0	30.0	5.0	5.0	30.0	5.0	5.0	30.0	5.0	5.0
[a]2.7	30.5	30.5	3.8	22.5	22.5	5.3	17.0	17.0	7.5	12.9	12.9
2.7	30.1	30.0	3.8	22.0	22.1	5.3	16.7	16.6	7.5	10.7	10.6
[b]2.2	38.0	38.5	3.1	28.3	28.3	4.4	21.2	21.2	6.2	16.4	16.4
2.2	43.1	43.0	3.1	31.5	31.6	4.4	23.9	23.9	6.2	15.3	15.2

[a] Values obtained with an average return speed of 23.8 cm s^{-1}.
[b] Values obtained with an average return speed of 16.6 cm s^{-1}.

on the catheter and inter-dwell distances of 0.5 cm and totaling 50 dwell positions with a total dwell time of 232.2 s. The prescribed dose at the surface of the prostate was also 10 Gy.

3. Results

3.1. Methodology validation

The discrete approximation for the source position while travelling was compared against a uniform distribution using a point source resulting in a maximum difference of 0.6% and 0.06% when using a resolution of 100 and 10 μm, respectively. The higher step resolution has been adopted to ensure that the methodology would not interfere with the final result. Once the spatial resolution was defined the transit dose component was calculated with the analytical method (equation (1)) and simulated with MC techniques for a 10 cm long linear catheter considering a source air-kerma strength of 40 700 U, as shown in table 2.

The simulation results were validated by the analytical method showing small differences due to rounded numbers when processing the TPS data, due to the simulation uncertainty component Type A ($k = 1$) of approximately 1% and due to the simplified approach which considers only the inverse square distance law. The transit dose component is proportional to the square root of the acceleration, i.e. the square root of the acceleration ratio of the microSelectron source (113 cm s^{-2} (Minamisawa *et al* 2010)) and the Varian GammaMed-Plus HDR source (55 cm s^{-2} (Wojcicka *et al* 1999)) is 1.43, which is the same as the ratio between the respective transit doses obtained independently employing both accelerations. Moreover, an approximation of the transit dose component can be obtained by comparing the time the source spends traveling inside the applicator and the total dwell time. For instance, for this applicator with 41 dwell positions, inter-dwell distance of 0.25 cm and a total dwell time of 76.0 s the dwell dose at the reference point is 510 cGy, while the transit time ($|a| = 113$ cm s^{-2}) is 4.25 s and the transit dose is 28.5 cGy, which is approximately 6% of the total dwell time and 6% of the dwell dose. Adding one more parallel catheter with the same number of dwell positions at the opposite side equidistants from the reference point, for

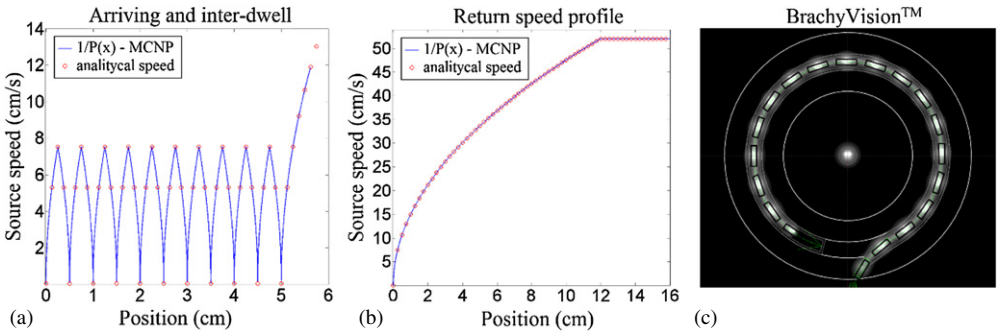

Figure 2. (a) Source instantaneous speed, derived from the source trajectory and dwell positions, for each discrete source position compared against analytical calculation for the source approaching the first dwell position at 5 cm and moving between the dwell positions (right to left) up to the last dwell position that was defined as the origin; (b) instantaneous speed validation for the source coming back to the safe; (c) BrachyVision™ ring applicator showing the dwell positions (black boxes) superimposed over a transit dose distribution without the dwell dose component.

the same prescription dose the total dwell time would remain the same, but the transit time would double (it is independent of total dose).

Figure 2 shows the last two steps of the validation process: (a) the inverse of the probability ($P(x)$), equal to the source instantaneous speed, of each discrete source position was compared against the analytical speed calculation (figures 2(a) and (b)) to validate the source speed profile calculate by the MATLAB algorithm; (b) the dose distribution considering only the transit component was exported as DICOM images to BrachyVision™ allowing a visualization of the applicator and its dwell positions over the transit dose distribution (figure 2(c)). This figure shows that the transit dose distribution for a uniform accelerated movement follows the applicator geometry and has a higher dose deposition near the dwell positions, due to the source slowing down.

3.2. Studied cases

The studied cases simulated using a uniform acceleration of 113 cm s^{-2} (Minamisawa *et al* 2010) are presented below and possible differences due to the speed profiles are discussed in section 3.3.

3.2.1. Gynecological cases. Case a with one central catheter has an average transit dose of 3.7 cGy or approximately (0.5 $\pm$ 0.1)% of the dwell dose at the dose prescription points showing a more homogenous dose ratio due to the symmetry of the case. The time correction was applied with an average dwell time reduction of 0.16 s per dwell position reducing the transit dose component to approximately (-0.1 ± 0.1)% of the dose at the prescription points.

The transit dose component for case b with four catheters varies according to the body regions and can be seen in figure 3 where the transit dose considering the instantaneous speed shows symmetrical behavior due to the uniformly distributed dwell positions while the dwell dose is higher on the right hand side of the applicator as can be seen by the isodoses in figure 3(a), which are a bit shifted to the right side.

The mean transit dose for case b is (1.8 $\pm$ 0.2)% of the dose at the prescription points, reaching 28.4 cGy using the instantaneous speed approach ($|a| = 113$ cm s^{-2}). A dwell time correction calculated using equation (3) resulted in an average dwell time reduction of 0.13 s

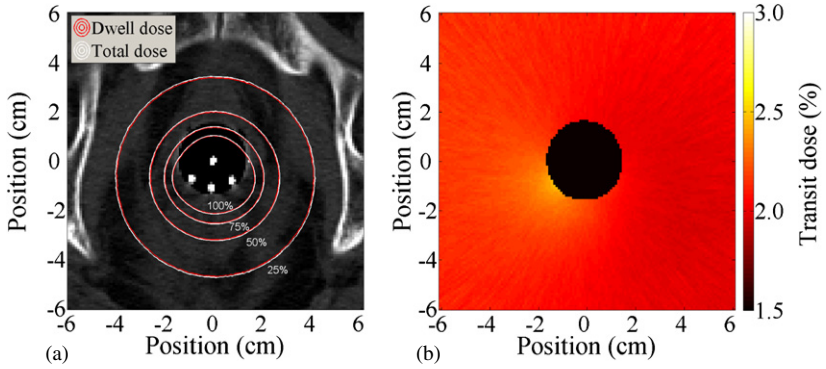

Figure 3. Gynecological case b (transverse plane): (a) isodoses obtained considering the dwell dose and the total dose, which corresponds to the transit dose added to the dwell dose distribution; (b) transit dose component as a percentage of the dwell dose without dwell time corrections. The dose inside the applicator (black circle) was not scored.

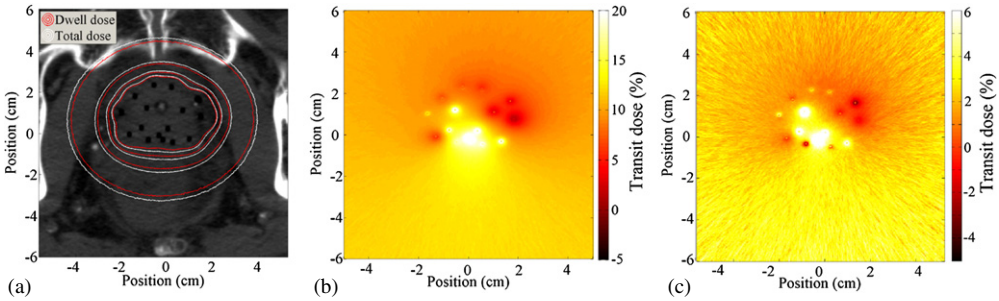

Figure 4. Prostate case c (transverse plane): (a) isodoses in a CT slice with source catheters indicated as black holes and with the prostate contour approximately equal to the innermost isodose contour; (b) the ratio in percentage between the transit dose and the dwell dose; (c) the ratio in percentage between the corrected transit dose and the dwell dose. (b) and (c) are shown using different scales.

per dwell position reducing the mean transit dose component effect to less than 0.1% of the dwell dose at the dose prescription points. The proposed time correction is the same for both gynecological cases since they employ the same inter-dwell distance and this reduces the transit dose component by approximately a factor of 4 for these cases. The dwell and transit dose are around 5% higher when assigning proper material compositions compared to using an infinite water medium (TG43-U1 formalism), but it does not affect the dose ratio. However, the dose difference is up to 7% at the prescription points when the TG43-U1 formalism is compared to the results obtained with proper material compositions and taking the transit dose into account together; this is mainly due to the air gap inside the applicator.

3.2.2. Prostate case. The transit dose component for prostate case c reaches up to 20% or 1.8 Gy at some regions that present several catheters close to each other (figure 4) with an average transit dose component (figure 4(b)) of 1.1 Gy or (11.1 $\pm$ 0.5)% of the dwell dose inside the prostate including the dose to the urethra. The regions outside the prostate are mainly composed of soft tissues and show differences within 1% when proper tissue densities and composition are employed, which does not have a significant impact on the dose

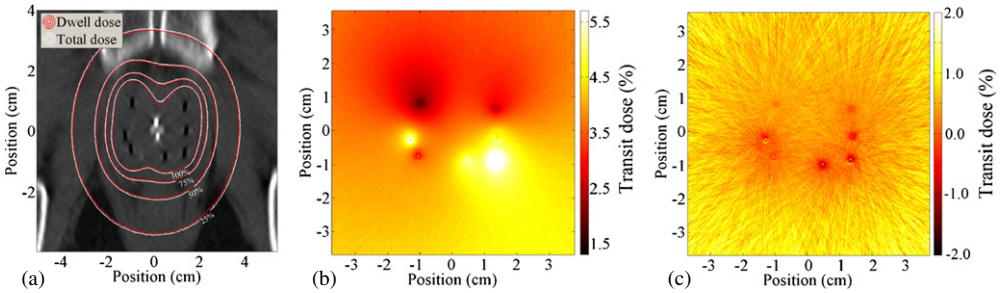

Figure 5. Prostate case d (transverse plane): (a) isodoses over a CT slice with the catheters corresponding to the boundaries of the prostate contour; (b) transit dose percentage compared against the dwell dose; (c) corrected transit dose percentage compared against the dwell dose. (b) and (c) are shown using different scales.

Table 3. Transit dose component for the studied cases considering speed profiles based on literature data in absolute dose and in percentage of the dwell dose. The average speed of 2.7 cm s^{-1} (gynecological cases) and 3.8 cm s^{-1} (prostate cases) were obtained with an acceleration of 113 cm s^{-2} for an inter-dwell distance of 2.5 mm (gynecological cases) and 5 mm (prostate cases).

	Studied cases			
	Average transit dose at the prescription points (cGy)/(%)		Average transit dose within the prostate volume (cGy)/(%)	
	Gynecological		Prostate	
	Case a	Case b	Case c	Case d
$v = 50$ cm s^{-1}	0.4/<0.1	3.0/0.2	13.7/1.4	10.2/0.6
$v = 30$ cm s^{-1}	0.7/0.1	5.0/0.3	22.8/2.3	17.0/1.0
$v = 2.7/3.8$ cm s^{-1}	4.1/0.6	31.0/2.0	115.0/11.7	64.8/4.1
$a = 113$ cm s^{-2}	3.7/0.5	28.4/1.8	108.8/11.1	60.3/3.8
$a = 77$ cm s^{-2}	4.5/0.6	34.4/2.2	131.8/13.4	73.1/4.6
$a = 55$ cm s^{-2}	5.3/0.7	40.7/2.6	155.9/15.9	86.4/5.4

distribution when compared against a uniform water medium and makes no difference in the transit dose ratio. Figure 4(c) shows the dose ratio with the dwell time correction, with an average difference 3.3 times lower than without correction, although the correction applied creates regions with dose differences between −5% and 6% at specific regions.

Prostate case d (figure 5(a)) has an average transit dose component (figure 5(b)) of (3.8 ± 0.2)% inside the prostate. Applying the dwell time correction reduced more than 2.9 times the transit dose effect inside the prostate (figure 5(c)), but with some regions inside the prostate showing differences up to 2.7% at specific points.

3.3. Speed profile effects

The transit dose evaluated using some speed profiles based on literature data is presented in table 3 for gynecological and prostate cases. The gynecological cases were evaluated considering the prescription points since the target contour was not available, whilst the prostate cases were evaluated using the prostate contour to obtain the average dose inside the volume.

Table 4. Transit time for the studied cases considering a uniform acceleration of $|a| = 77$ cm s^{-2} including the time correction applied. The mean transit dose was obtained considering the whole CT volume.

	Total dwell time (s)	Total transit time (s)	Time correction (s)		Transit time (%)	[a]Mean transit dose (%)	[b]Mean transit dose (%)
			This study (equation (3))	Palmer and Mzenda (2009) (equation (2))			
Case a	414.4	2.2	2.7	3.3	0.5	0.5	−0.1
Case b	555.8	12.5	12.8	19.7	2.3	2.3	<0.1
Case c	200.9	27.8	19.4	20.1	13.8	13.8	4.1
Case d	232.2	12.4	8.7	9.0	5.3	5.6	1.9

[a] Without time correction.
[b] With time correction.

3.4. Dwell time correction

The mean transit dose percentage over the volume can be estimated by calculating the total transit time of the source inside the catheter and the total dwell time, as presented in table 4. This is equivalent to the transit dose percentage averaged within the whole volume. The transit time was calculated considering an acceleration of $|a| = 77$ cm s^{-2} to compare the time correction adopted in this study with those obtained using equation (2) (Palmer and Mzenda 2009).

4. Discussion

The transit dose component is case specific ranging from negligible ($\leqslant$0.5%) for a gynecological case with one catheter up to 13.8% for the average transit dose within the whole CT volume for a prostate case considering a uniform acceleration $|a| = 77$ cm s^{-2}. These observed differences were also dependent on the evaluated region since the dwell dose is higher near the target volume and negligible far away from it. The transit dose component may represent the majority of the delivered dose in some regions far away from the target.

The gynecological case with one catheter employed prescription points at 0.5 cm from the surface of the applicator which is 2.25 cm away from the dwell positions resulting in long dwell times which leads to a negligible transit dose component relative to the dwell dose. However, the transit component may not be negligible for other similar cases. For instance, the transit component for the gynecological case with four catheters is approximately four times higher than the first case due to the number of catheters. Even larger differences were observed between the intracavitary and the interstitial prostate cases since the latter modality has much lower dwell times than the gynecological cases due to the proximity of the treated region. Moreover, the evaluated prostate cases use several catheters (up to 16) which, in general, results in longer travel times leading to a more significant transit dose component.

Significant dose differences were also observed between the interstitial cases. The prostate case d was performed using a more uniform catheter and dwell position distribution inside the prostate and with less than half the number of catheters and dwell positions than in case c. Due to these differences the transit dose component inside the prostate volume in case d is approximately three times lower than in case c. Differences between the cases can be easily visualized by comparing the source travel time and the total dwell time presented in table 4, which also provides an estimate of the average transit dose.

Although an estimate of the average transit dose can be obtained using the relationship between travel and dwell times, a uniform acceleration results in transit dose hot spots near the dwell positions and lower transit doses in between them leading to a complex transit dose

distribution. This complexity level depends on the speed profile, number of catheters, dwell positions and their spatial distribution. These factors associated with a limited number of dwell positions do not allow a full transit dose compensation just by reducing the dwell time. This approach may lead to cold and hot spots since the time correction necessary to reduce the transit dose near the dwell positions may result in an underdose in other regions. Nevertheless, the applied dwell time corrections reduced considerably the transit dose component for our cases and produced more homogeneous distributions when using an accurate speed profile (figure 4).

Tenfold differences can be observed between the speed scenario for the microSelectron (an average speed of 50 cm s^{-1}) and the worst scenario (uniform acceleration of $|a| = 55$ cm s^{-2}) for all cases. The average transit dose inside the prostate volume obtained using an average or instantaneous variable speed with the same acceleration value were equivalent. However, these approaches lead to different transit dose distributions since the transit dose near the dwell positions is much higher using the latter approach due to the source slowing down near the dwell positions.

The source travel time between the dwell positions is the main component of the transit dose within the target volume, which was the main interest in this study. However, when the acceleration is assumed uniform for the transit dose calculation a maximum source speed should be defined, otherwise the source could attain unrealistic speeds when exiting from the safe or returning to it. This study used 52 cm s^{-1} as the maximum source speed; different speed values showed no significant difference for the transit dose component for the studied cases due to the assumed trajectory length. These trajectories imported from the treatment plan have limited lengths since they cover mainly the region with dwell positions due to its clinical relevance. The source, in general, does not reach its maximum speed close to the target; this happens only over a few centimeters far away from the target volume.

5. Conclusion

The transit dose for ^{192}Ir HDR brachytherapy treatments can be significant, reaching more than 1.8 Gy and representing up to 20% of the dwell dose for a specific region of the prostate case (figure 4(b)) analyzed in this study. The transit dose was found to be more significant for the interstitial cases analyzed since they have lower dwell times due to the proximity between the dwell positions and the tissue. Although the literature data do not agree, the source speed seems to be low enough to produce significant effects in the dose distribution, which should be taken into account (Minamisawa *et al* 2010, Palmer and Mzenda 2009, Wojcicka *et al* 1999, Wong *et al* 2001). The simple approach adopted here to reduce the transit dose component is approximately equivalent to the one adopted by Palmer and Mzenda (2009) for $|a| = 77$ cm s^{-2}, reducing significantly the transit dose component with the advantage of taking into account different acceleration values. However, complex distributions of catheters and dwell positions combined with the acceleration effect can lead to hot and cold spots in the total dose distribution, which should be analyzed for each case using an accurate source speed profile. This should be included in the TPS to reduce the transit dose effects using algorithms that consider a more accurate source movement model, which are beyond the scope of this work.

Acknowledgments

This work was partially supported by *Fundação de Amparo à Pesquisa do Estado de São Paulo* (FAPESP), grant numbers 2011/01913-4, 2011/23765-7 and 2011/22778-8. This work is supported by grant #2011-700810 of the Canadian Cancer Society Research Institute (CCSRI).

GL was supported by the Natural Sciences and Engineering Research Council of Canada (NSERC) and by the O'Brien Foundation. BR was supported by a Marie Curie Reintegration Grant (grant agreement no. PIRG05-GA-2009-247878 from FP7-PEOPLE-2009-RG).

References

Afsharpour H, Landry G, D'Amours M, Enger S, Reniers B, Poon E, Carrier J-F, Verhaegen F and Beaulieu L 2012 ALGEBRA: ALgorithm for the heterogeneous dosimetry based on GEANT4 for BRAchytherapy *Phys. Med. Biol.* **57** 3273–80

Bastin K T, Podgorsak M B and Thomadsen B R 1993 The transit dose component of high dose rate brachytherapy: direct measurements and clinical implications *Int. J. Radiat. Oncol. Biol. Phys.* **26** 695–702

Beaulieu L, Tedgren A C, Carrier J F, Davis S D, Mourtada F, Rivard M J, Thomson R M, Verhaegen F, Wareing T A and Williamson J F 2012 Report of the Task Group 186 on model-based dose calculation methods in brachytherapy beyond the TG-43 formalism: current status and recommendations for clinical implementation *Med. Phys.* **39** 6208–36

Briesmeister J F 2008 *MCNP: a general Monte Carlo N-particle transport code,* version 5 Los Alamos Scientific Laboratory, Los Alamos, NM

Calcina C S G, Almeida A, Rocha J R O, Abrego F C and Baffa O 2005 Ir-192 HDR transit dose and radial dose function determination using alanine/EPR dosimetry *Phys. Med. Biol.* **50** 1109–17

Daskalov G M, Löffler E and Williamson J F 1998 Monte Carlo-aided dosimetry of a new high dose-rate brachytherapy source *Med. Phys.* **25** 2200–8

Fonseca G P, Rubo R A, Minamisawa R A, dosSantos G R, Antunes P C G and Yoriyaz H 2013 Determination of transit dose profile for a ^{192}Ir HDR source *Med. Phys.* **40** 051717

ICRP 1975 Report on the Task Group on Reference Man *ICRP Publication No. 23* (Pergamon, Oxford: International Commission on Radiological Protection)

Minamisawa R A, Rubo R, Seraide R M, Rocha J R O and Almeida A 2010 Direct measurement of instantaneous source speed for a HDR brachytherapy unit using an optical fiber based detector *Med. Phys.* **37** 5407–11

Nath R, Anderson L L, Luxton G, Weaver K A, Williamson J F and Meigooni A S 1995 *AAPM Technical Report* 51: *Dosimetry of Interstitial Brachytherapy Sources: Recommendations of the AAPM Radiation Therapy Committee Task Group No.* 43 *Med. Phys.* **22** 209–34

Palmer A and Mzenda B 2009 Performance assessment of the BEBIG MultiSource® high dose rate brachytherapy treatment unit *Phys. Med. Biol.* **54** 7417–34

Perez-Calatayud J, Granero D and Ballester F 2004 Phantom size in brachytherapy source dosimetric studies *Med. Phys.* **31** 2075–81

Petrokokkinos L, Zourari K, Pantelis E, Moutsatsos A, Karaikos P, Sakelliou L, Seimenis I, Georgiou E and Papagiannis P 2011 Dosimetric accuracy of a deterministic radiation transport based ^{192}Ir brachytherapy treatment planning system. Part II: Monte Carlo and experimental verification of a multiple source dwell position plan employing a shielded applicator *Med. Phys.* **38** 1981–92

Planning system manual ONCENTRA® MasterPlan v3.3 Physics and Algorithms Ref. 192.718ENG-04

Poon E, Le Y, Williamson J F and Verhaegen F 2008 BrachyGUI: an adjunct to an accelerated Monte Carlo photon transport code for patient-specific brachytherapy dose calculations and analysis *J. Phys.: Conf. Ser.* **102** 012018

Rivard M J, Coursey B M, DeWerd L A, Hanson W F, Huq M S, Ibbott G S, Mitch M G, Nath R and Williamson J F 2004 *Technical Report* 84: *Update of AAPM Task Group No.* 43 *Report*: *A Revised AAPM Protocol for Brachytherapy Dose Calculations Med. Phys.* **31** 633–74

Sahoo N 2001 Measurement of transit time of a remote after-loading high dose rate brachytherapy source *Med. Phys.* **28** 1786–90

Taylor R E P and Rogers D W O 2008 EGSnrc Monte Carlo calculated dosimetry parameters for ^{192}Ir and ^{169}Yb brachytherapy sources *Med. Phys.* **35** 4933–44

Venselaar J 2013 Standard technology in brachytherapy *Comprehensive Brachytherapy: Physical and Clinical Aspects* (Boca Raton, FL: CRC Press) pp 9–28

Wojcicka J B, Yankelevich R, Trichter F and Fontanla D P 1999 Comparison of the transit dose components and source kinematics of three high dose rate afterloading systems *Med. Dosim.* **24** 61–5

Wong T P Y, Fernando W, Johnston P N and Bubb I F 2001 Transit dose of an Ir-192 high dose rate brachytherapy stepping source *Phys. Med. Biol.* **46** 323–31